Two dimensional Navier Stokes equations

Rinat Faizulin

1 Mathematical problem

1.1 Physical domain

The domain if defined by space domain $\Omega_{\boldsymbol{x}} = [0, L] \times [0, H]$ and time domain $\Omega_t = [0, t_f]$, where $\boldsymbol{x} = (x, y)$ is the space coordinates and t is the time. Figure 1 displays the flow domain's schematic representation.

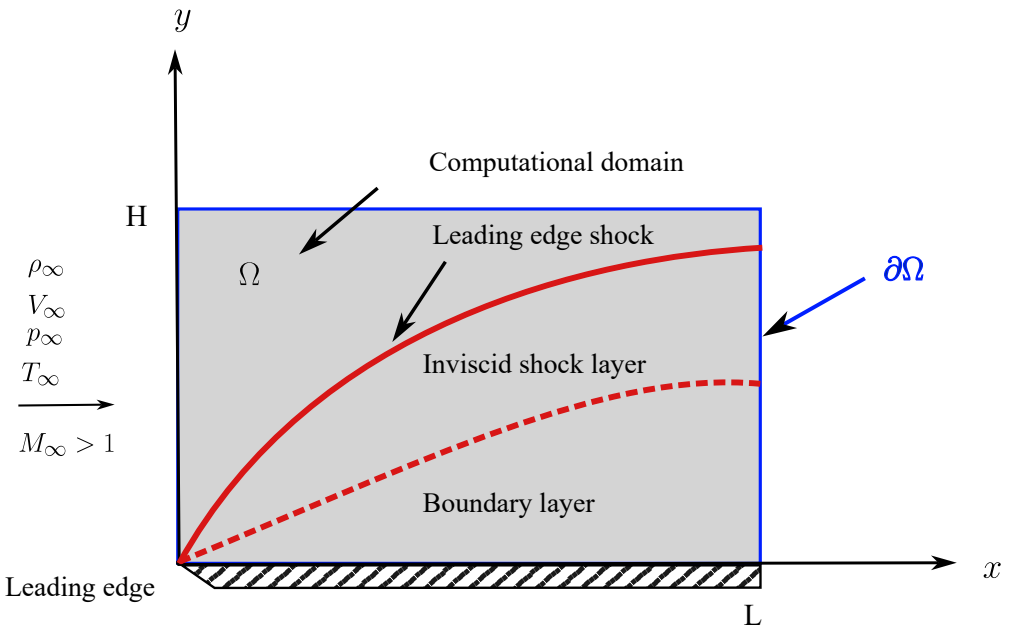

Figure 1. *Illustration of the physical domain.*

1.2 The Governing Flow Equations

The two-dimensional Navier Stokes equations consist of three primary equations: the continuity equation, the momentum equation and the energy equation.

The continuity equation:

$$\frac{\partial \rho}{\partial t} + \frac{\partial (\rho u)}{\partial x} + \frac{\partial (\rho v)}{\partial y} = 0, \tag{1}$$

The momentum equations:

$$\frac{\partial (\rho u)}{\partial t} + \frac{\partial (\rho u^2 + p - \tau_{xx})}{\partial x} + \frac{\partial (\rho uv - \tau_{yx})}{\partial y} = 0, \tag{2}$$

$$\frac{\partial (\rho v)}{\partial t} + \frac{\partial (\rho uv - \tau_{xy})}{\partial x} + \frac{\partial (\rho v^2 + p - \tau_{yy})}{\partial y} = 0, \tag{3}$$

where, shear stress is defined as follows:

$$\tau_{xy} \;=\; \tau_{yx} \;=\; \mu\left(\frac{\partial u}{\partial y} \;+\; \frac{\partial v}{\partial x}\right), \tag{4}$$

with normal stress components are described as following:

$$\tau_{xx} \;=\; \lambda(\,\nabla\cdot V\,) \;+\; 2\mu\frac{\partial u}{\partial x}, \tag{5}$$

$$\tau_{yy} \;=\; \lambda(\,\nabla\cdot V\,) \;+\; 2\mu\frac{\partial v}{\partial y}, \tag{6}$$

where, the coefficient λ is related to viscosity μ by the equation $\lambda \;=\; -\frac{2}{3}\mu$.

The Energy equation:

$$\frac{\partial(E_t)}{\partial t} \;+\; \frac{\partial[\,u(\,E_t \;+\; p\,) \;+\; q_x \;-\; u\tau_{xx} \;-\; v\tau_{xy}\,]}{\partial x} \;+\; \frac{\partial[\,v(\,E_t \;+\; p\,) \;+\; q_y \;-\; u\tau_{yx} \;-\; v\tau_{yy}\,]}{\partial y} \;=\; 0\,, \tag{7}$$

the components of the heat flux vector in the horizontal x and vertical y directions expressed as:

$$q_x \;=\; -k\frac{\partial T}{\partial x}, \quad q_y \;=\; -k\frac{\partial T}{\partial y}, \tag{8}$$

with the total energy E_t defined as:

$$E_t \;=\; \rho\left(e \;+\; \frac{V^2}{2}\right) \tag{9}$$

At this stage, the system comprises four fundamental equations: continuity, x Momentum, y Momentum, and energy. These equations introduce nine unknowns into the system: density ρ, horizontal velocity u, vertical velocity v, magnitude of velocity $|V|$, pressure p, temperature T, internal energy e, dynamic viscosity μ, and thermal conductivity k. To establish a closed system, an additional five equations are required. They are detailed below:

1. The ideal gas law is an equation that relates pressure p, density ρ, temperature T:

$$p \;=\; \rho RT \tag{10}$$

2. Considering calorically perfect air, we can use an equation that relates internal energy e to temperature T:

$$e \;=\; c_v T \tag{11}$$

3. The relationship between the horizontal velocity u and vertical velocity v is determined through the magnitude of velocity $|V|$:

$$|V| \;=\; \sqrt{u^2 \;+\; v^2} \tag{12}$$

4. When estimating dynamic viscosity μ, often in the context of a calorically ideal gas, the Sutherland's law is common practice:

$$\mu \;=\; \mu_0\left(\frac{T}{T_0}\right)^{\frac{3}{2}}\frac{T_0 \;+\; 110}{T \;+\; 110} \tag{13}$$

5. An additional equation is required to close the system. Assuming a constant Prandtl number approximately equal to 0.71, thermal conductivity k can be determined in terms of dynamic viscosityand specific heat at constant pressure:

$$Pr \;=\; 0.71 \;=\; \frac{\mu c_p}{k} \tag{14}$$

The system of equations is now considered closed, encompassing a total of nine equations that correspond to an equal number of unknowns.

1.3 Initial and Boundary conditions

For initial conditions, the values of the flow properties are set equal to their corresponding freestream values.

$$\begin{aligned} u(\boldsymbol{x},t) &= u_\infty\,, \quad v(\boldsymbol{x},t) = v_\infty\,, \quad \boldsymbol{x} \in \Omega_{\boldsymbol{x}}, \quad t = 0 \\ p(\boldsymbol{x},t) &= p_\infty\,, \quad T(\boldsymbol{x},t) = T_\infty \end{aligned} \tag{15}$$

The boundary conditions are schematically represented in Figure 2. For further modeling, $\Omega_t^\star = \Omega_t \setminus \{0\}$ is defined.

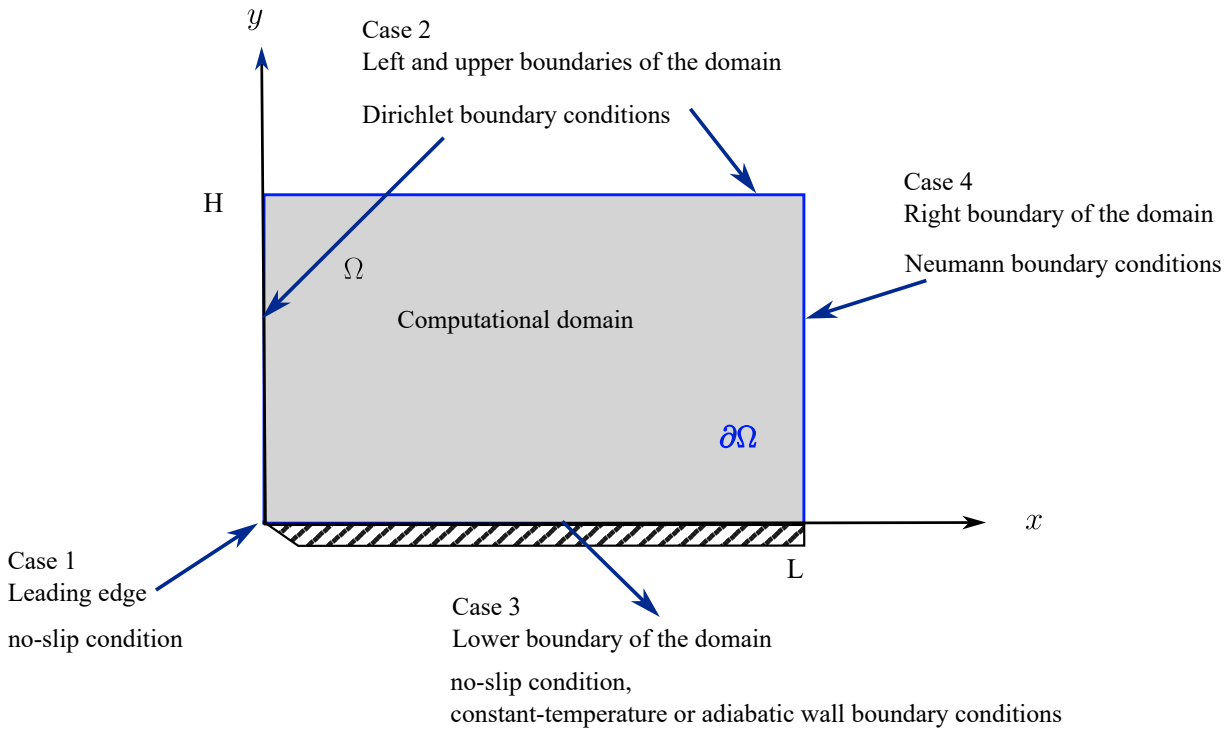

Figure 2. *Illustration of the boundary conditions.*

Case 1

$$\begin{aligned} u(\boldsymbol{x},t) &= 0\,, \quad v(\boldsymbol{x},t) = 0\,, \quad \boldsymbol{x} \in [0] \times [0], \quad t \in \Omega_t^\star \\ p(\boldsymbol{x},t) &= p_\infty\,, \quad T(\boldsymbol{x},t) = T_\infty \end{aligned} \tag{16}$$

For the Case 1, Dirichlet boundary conditions are set at the leading edge, where horizontal velocity u and vertical velocity v are equal to zero, which physically ensures the absence of sliding, and the temperature T and the pressure p correspond to the freestream values.

Case 2

$$\begin{aligned} u(\boldsymbol{x},t) &= u_\infty\,, \quad v(\boldsymbol{x},t) = v_\infty\,, \quad \boldsymbol{x} \in [0] \times (0,H], \quad t \in \Omega_t^\star \\ p(\boldsymbol{x},t) &= p_\infty\,, \quad T(\boldsymbol{x},t) = T_\infty \end{aligned} \tag{17}$$

$$
\begin{aligned}
u(\boldsymbol{x},t) &= u_\infty\,, \quad v(\boldsymbol{x},t) = v_\infty\,, \quad \boldsymbol{x} \in [0,L]\times[H], \quad t \in \Omega_t^\star \\
p(\boldsymbol{x},t) &= p_\infty\,, \quad T(\boldsymbol{x},t) = T_\infty
\end{aligned}
\tag{18}
$$

On the left and upper boundaries of the domain (Case 2), excluding the leading edge, Dirichlet boundary conditions are set, where the values for horizontal velocity u, vertical velocity v, temperature T, and pressure p correspond to the freestream values.

Case 3

$$
\begin{aligned}
u(\boldsymbol{x},t) &= 0\,, \quad v(\boldsymbol{x},t) = 0\,, \quad \boldsymbol{x} \in (0,L]\times[0], \quad t \in \Omega_t^\star \\
\frac{\partial p(\boldsymbol{x},t)}{\partial y} &= 0\,, \quad T(\boldsymbol{x},t) = T_w
\end{aligned}
\tag{19}
$$

For the lower boundary of the domain (Case 3), excluding the leading edge, Dirichlet boundary conditions are set for horizontal velocity u, vertical velocity v, temperature T, where $u = v = 0$ (no-slip conditions), and temperature T is equal to the T_w (wall temperature), which is constant-temperature wall boundary. For the pressure p, the Neumann boundary condition is set equal to zero. To study the variation of the flow field properties, the adiabatic wall boundary condition is considered, which means the Neumann boundary condition is set equal to zero: $\frac{\partial T(\boldsymbol{x},t)}{\partial y} = 0$.

Case 4

$$
\begin{aligned}
\frac{\partial u(\boldsymbol{x},t)}{\partial x} &= 0\,, \quad \frac{\partial v(\boldsymbol{x},t)}{\partial x} = 0\,, \quad \boldsymbol{x} \in [L]\times(0,H), \quad t \in \Omega_t^\star \\
\frac{\partial p(\boldsymbol{x},t)}{\partial x} &= 0\,, \quad \frac{\partial T(\boldsymbol{x},t)}{\partial x} = 0
\end{aligned}
\tag{20}
$$

For the right boundary of the domain (Case 4), not including lower and upper boundaries, for horizontal velocity u, vertical velocity v, temperature T, pressure p, the Neumann boundary conditions is set equal to zero.

2 Numerical test

The case study considers adiabatic and constant-temperature boundary wall cases.
Table 1 contains a list of freestream values, the ratio $\frac{T_w}{T_\infty}$ was set equal to 1.

Table 1. *Input Data for the freestream values.*

$\rho_\infty\ [kg\cdot m^{-3}]$	$u_\infty\ [m\cdot s^{-1}]$	$v_\infty\ [m\cdot s^{-1}]$	$p_\infty\ [kg\cdot m^{-1}\cdot s^{-2}]$	$T_\infty\ [K]$	$M_\infty\ [-]$
1.22	1361	0	101325	288.16	4

In Table 2 there is listed thermodynamic characteristics and reference values for dynamic viscosity and temperature for both cases.

Table 2. *Input Data for the thermodynamic characteristics and reference values.*

$c_v\ [J\cdot kg^{-1}\cdot K^{-1}]$	$c_p\ [J\cdot kg^{-1}\cdot K^{-1}]$	$R\ [J\cdot kg^{-1}\cdot K^{-1}]$	$Pr\ [-]$	$\mu_0\ [kg\cdot m^{-1}\cdot s^{-1}]$	$T_0\ [K]$
717	1005	287	0.71	1.7894×10^{-5}	288.16

The length of the plate LHORI, vertical height of the domain LVERT, step sizes in x and y directions, grid size N, Reynolds Re_L and CFL numbers are listed in Table 3.

Table 3. *Input Data for the space, Reynolds and CFL numbers.*

LHORI $[m]$	LVERT $[m]$	Δx $[m]$	Δy $[m]$	N $[-]$	Re_L $[-]$	CFL $[-]$
10^{-5}	8.18×10^{-6}	1.25×10^{-8}	1.02×10^{-8}	800×800	931.91	0.1

3 Results

Figure 3 shows the comparison of normalized flow-field properties for horizontal velocity $\frac{u}{u_\infty}$ $[-]$, pressure $\frac{p}{p_\infty}$ $[-]$ and temperature $\frac{T}{T_\infty}$ $[-]$ for the RK4 method as red curves and the Mac Cormack method as green curves for the case of constant temperature wall at the trailing edge. The result shows agreement between the RK4 and Mac Cormack methods at the trailing edge for the constant case.

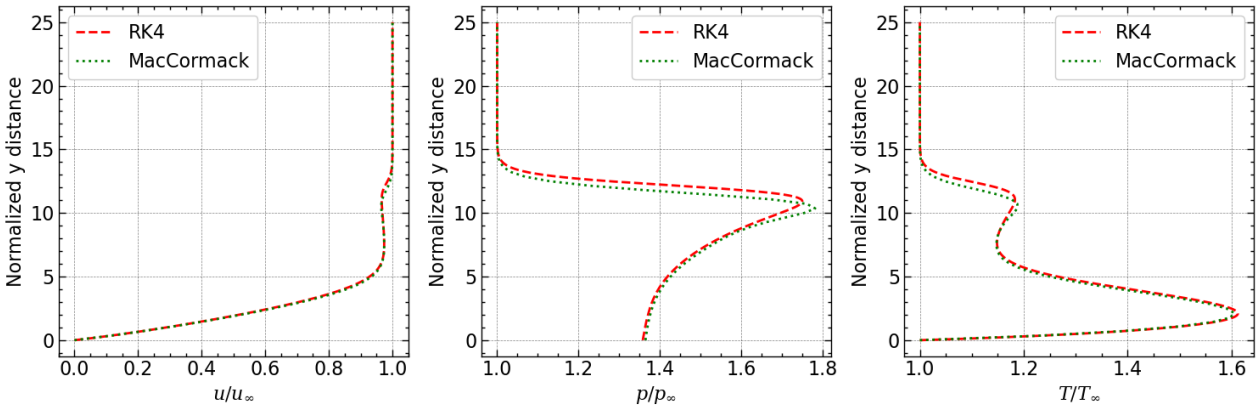

Figure 3. *Normalized horizontal velocity, pressure and temperature profiles for the constant wall temperature case at the trailing edge, RK4 as red curves and Mac Cormack as green curves from left to right.*

The normalized profiles of horizontal velocity, pressure and temperature for the adiabatic wall temperature case at the trailing edge are displayed in Figure 4. The RK4 method is represented by red curves, and the Mac Cormack method is represented by green curves. As can be observed for the horizontal velocity, the shock formation differs when compared to the constant-temperature wall case. Under adiabatic conditions, it is observed that the overall pressure increase compared to the constant-temperature wall condition. The increase in temperature is much higher for adiabatic case, also temperature within the boundary layer is roughly three times higher. As we can see, RK4 and Mac Cormack methods give slightly different results at the trailing edge for the adiabatic case.

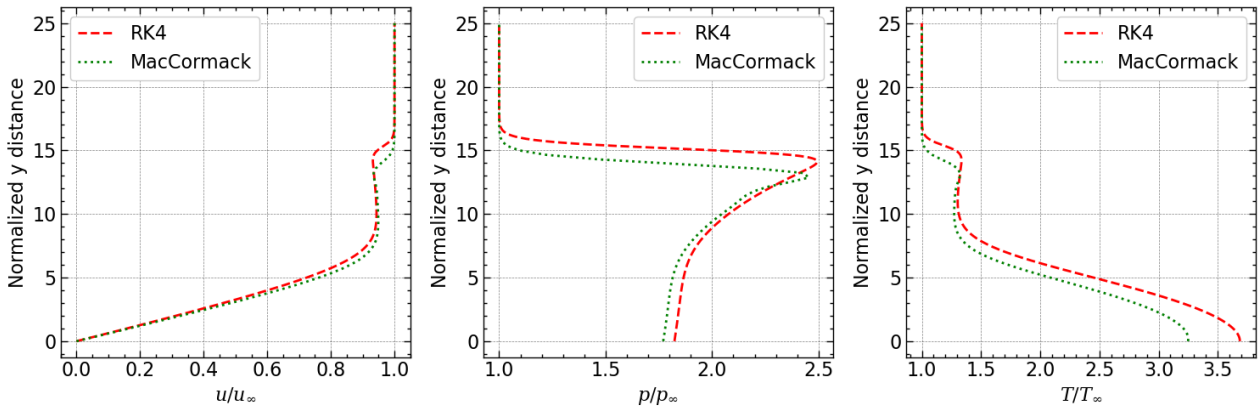

Figure 4. *Normalized horizontal velocity, pressure and temperature profiles for the adiabatic wall temperature case at the trailing edge, RK4 as red curves and Mac Cormack as green curves from left to right.*

In Figure 5 there is presented a comparison of the Mach number M contours over the entire domain for the constant case of wall temperature, where the RK4 method is shown on the left and the Mac Cormack method is shown on the right, as can be observed the methods give similar results for the entire domain for the constant case.

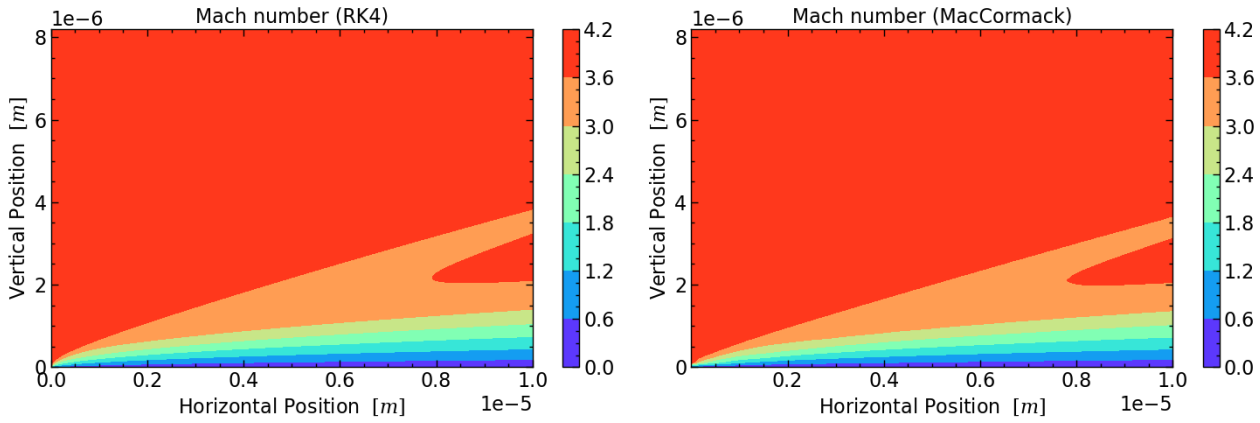

Figure 5. *Distribution of the Mach number over the entire domain, RK4 method on the left and Mac Cormack method on the right for the constant temperature wall case.*

Figure 6 illustrates the contours for the Mach number M for the adiabatic case over the entire domain, where the RK4 method is on the left and the Mac Cormack method is on the right. It can be seen how the adiabatic case affects the shock wave compared to the constant case. The methods give a similar result throughout the domain, although they differed at the trailing edge for the one-dimensional profiles as shown in Figure 4.

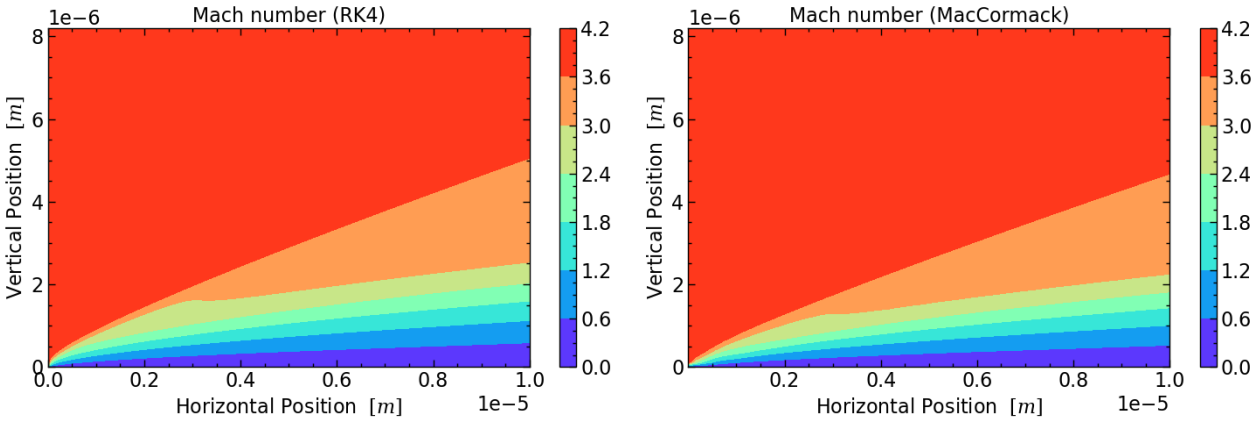

Figure 6. *Distribution of the Mach number over the entire domain, RK4 method on the left and Mac Cormack method on the right for the adiabatic temperature wall case.*